Studying Gravitational Waves from Exceptional Binary Black Hole Merger Events

LIGO SURF 2020 Second Interim Report

Jennifer Sanchez

Physics Department, California State University, Fullerton

Mentors: Dr. AlanWeinstein and Dr. Colm Talbot
LIGO Laboratory, Physics Department, California Institute of Technology
(Dated: July 31, 2020)

Advanced LIGO and Advanced Virgo have confidently detected gravitational wave signals from ten binary black hole mergers and one merger from a binary neutron star. Each observation contains encoded information about the physical properties of the binary system. As the detectors continue to improve their sensitivity, these developments will allow us to detect rarer systems and make more confident statements regarding their source properties. In order to fully characterize the gravitational wave observations, we rely on numerical and analytical models that approximate the signal waveforms from the emitted source as specified by the source parameters (masses, spins, sky location, etc). The dominant emission frequency of gravitational waves from compact binary coalescence is at twice the orbital frequency; however, recently published events have demonstrated subdominant higher order harmonic contributions. The primary focus of this study is to explore higher order modes in gravitational wave signals with newly improved signal models.

I. INTRODUCTION

Black hole binaries, along with other compact binaries, are responsible for the gravitational waves that have been detected by the LIGO Scientific Collaboration [1] and Virgo [2]. Since 2015, the year in which the first gravitational wave was detected, there have been nine additionally confirmed gravitational waves from binary black hole mergers, one merger from a binary neutron star, and 56 candidate detections of gravitational wave signals [3]. The current operational detectors are only able to observe the closest and loudest sources that exist in the local universe. Now that gravitational waves can be detected and analyzed, this is only the beginning for gravitational wave science.

During the third observing run (O3) of Advanced LIGO and Advanced Virgo, all three interferometers operated at unprecedented sensitivity [4]. With the observations of 67 gravitational wave signals, the need for accurate models of the emitted sources is essential [5]. Observations made during the O3 have provided the first evidence for binaries with unequal mass and misaligned spins [6].

Parameters describing the merging binaries are inferred using Bayesian inference by comparing waveform templates ("approximants") to the data. Earlier parameter waveform families did not include higher order modes; however, the recent observations require waveform models including higher-order emission modes. Not only will these models provide us with information regarding the inspiral, merger, and ringdown of the source, but will also allow tests of general relativity [7], measurements of the underlying population of compact objects [8] and the expansion history of the Universe [9].

In this report, we will be discussing the properties of the events called GW190412 and GW190814 which were observed by both Advanced LIGO and Advanced Virgo detectors [6] [10]. Their signal waveforms included its signature dominant quadrupole radiation; however, they also contained *detectable* higher harmonics which will provide us with a greater insight to the dynamics of coalescing binary black holes. The focus of this study is on events like GW190412 and GW190814.

II. METHODS

The first three weeks were spent on learning how to use LIGO and Virgo strain data along with their affiliated software libraries. The programming exercises provided by the GW Open Data Workshop #3 [11] have allowed me to utilize the gravitational wave data as well as their software tools. Upon completing all of the tutorials, I began to learn how to use Bilby [12], a Bayesian inference library for gravitational-wave astronomy. Through the tutorials, I was able to run parameter estimations on different astrophysical systems. I have also been learning the dynamics of surrogate modeling, and how to use the newest surrogate model, NRSur7dq4 (Numerical Relativity Surrogate with 7-parameters and mass ratio, q, ranging from one to four) [13].

More recently, I have familiarized myself with PyCBC [14], a software package used to analyze gravitational waves. I have been comparing different higher-mode waveform models using parameters from GW190412. This has led me to estimate the differences between the waveform models and determine how consistent the results are when using multiple posterior samples for source

properties [15].

A. Source Properties

The source properties we have been studying prior to O3 included: masses (m_1 and m_2), spins of the black holes in the binary ($\vec{S_1}$ and $\vec{S_2}$), the sky location, luminosity distance (D_L), binary orbital orientation, time (t_c) and phase (ϕ_c) of coalescence. All of these properties comprise to a total of 15 parameters. Specifying these parameters allows one to predict the signal waveform that may be present in the detector network data.

Gravitational waves are transverse waves that have two independent polarization states denoted as h_+ and $h_\times$, where $h_\times$ has its principle axis rotated $45°$ with respect to h_+ [16]. With these two polarizations at hand, we can write the strain of the gravitational wave as the complex quantity, $h = h_+ - ih_\times$ [17]. According to the works of pioneering scientists, another fundamental property of gravitational waves from compact binaries is that they are quadrupolar. While gravitational radiation often includes the lowest order radiation term, the quadrupole radiation, there are predictions that include higher multipoles [18]. However, higher multipoles, which are terms above the dominant, quadrupolar term, are particularly complex to infer from a gravitational wave signal produced by near equal mass binaries [6].

Recently, signal waveform families have been extended to include higher order modes. The dominant mode is $(l, m) = (2, 2)$ described by a spin-weighted spherical harmonic, $_{-2}Y_{lm}(\theta, \phi)$, where θ and ϕ are the emission angles toward the observer relative to the orbital angular momentum, ℓ. We can describe the multipolar decomposition as:

$$h_+ - ih_x = \sum_{\ell=2}^{\infty} \sum_{m=-\ell}^{\ell} \frac{h(t, \lambda)}{D_L} {}_{-2}Y_{\ell m}(\theta, \phi) \qquad (1)$$

where t denotes the time, λ represents the intrinsic parameters such as the black hole's masses and spins, and D_L represents the luminosity distance from the observer. Lastly, we recognize that, $h = h_+ - ih_\times$ is in the form of a complex sinusoidal, $cos(\omega t) - isin(\omega t)$ or similarly $e^{-i\omega t}$.

The event's mass ratio, q, is an important factor to consider since it affects the geometry of the source. General relativity predicts that when the masses of the binary are increasingly unequal, the higher order multipoles are increasingly important.

Another contributor to higher multipoles is the orientation of the source. Higher order multipoles are more prominent when θ is different from 0 or π, also said to be "face on." As a result to the degeneracy between θ and D_L, higher multipoles allow us to break this degeneracy which allows us to tighten constraints on the two [6].
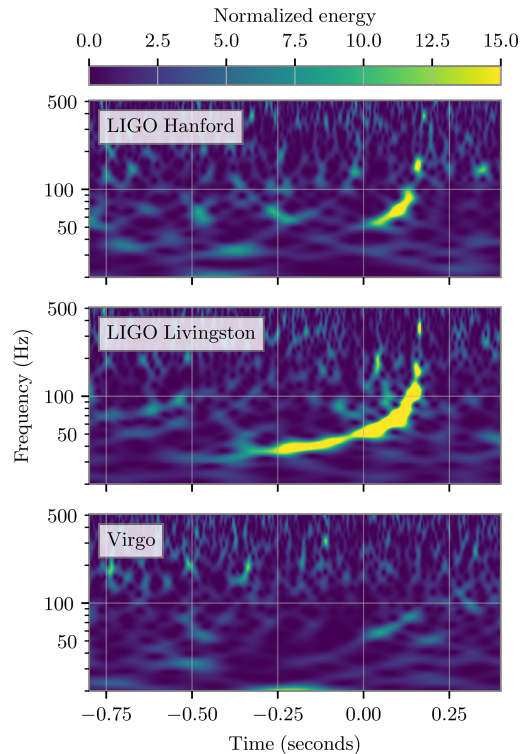

FIG. 1. Spectrogram of GW190412 in LIGO Hanford (top), LIGO Livingston (middle), and Virgo (bottom). The x-axis represents time while the y-axis represents the frequency of the gravitational wave signal. In this time-frequency representation, we show the energy given a specific frequency at a specific time. The increase in frequency and energy over time is a product of the inspiraling black holes followed by their merger.

B. Higher multipoles

It is critical to have theoretical models of a gravitational wave signals that agree with the measurements made from Advanced LIGO and Virgo. Typically, these models include the dominant $(l, m) = (2, 2)$ mode; however, this is not always the case. When the sources have a mass ratio close to one, these models are sufficient to analyze the source parameters of the system, such as distance and inclination. However, when the black hole binary contains an unequal mass ratio, subdominant multipole models may be remarkably more accurate.

Shown in Fig. 1, we can see the strain data from GW190412, the fractional change in displacement between two nearby masses due to the gravitational wave, taken by the three detectors. The time-frequency representation of GW190412 shows the signal to noise ratio (SNR, informally referred to as the "loudness") of the event in each detector. Despite the fact that the detectors are thousands of kilometers away from one another, we can definitively see that the signal is present in all three which implies that the source has an astrophysical
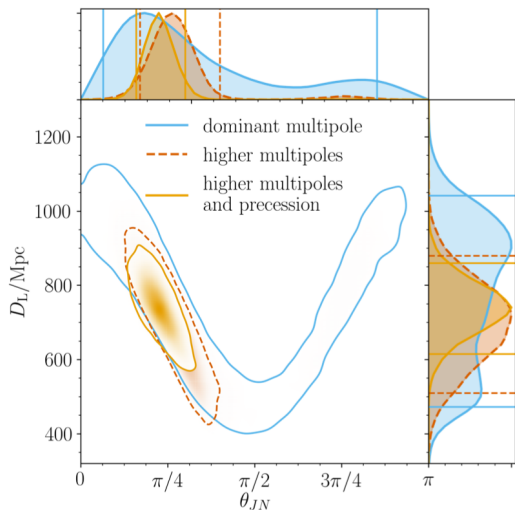
FIG. 2. Posterior distribution of GW190412 luminosity dsitance (D_L) and inclinatoin (θ). We see that by using models that include the dominant multipole, higher mulitpoles, and higher multipoles and precession, we are able to constrain D_L and θ. Degeneracy breaks when higher order modes are included which allows us to improve our accuracy.

origin rather than local detector noise [6].

What makes this event so unique is the notable asymmetry of the black hole masses, that is – one of the black hole's mass is roughly three times heavier than the other [6]. This makes GW190412 a favorable system for identifying the presence of higher order modes. Previously, nearly all detected binary systems were consistent with having zero net aligned spin; however, we found that GW190412 has significant net positive aligned spin χ_{eff} [6]. On account of the unequal mass ratio, we can apply a constraint on the spin of the larger black hole. Making use of higher order modes in the model waveforms will allow us to make more precise measurements of all the parameters including the distance and inclination of the system, also shown in Fig. 2. General relativity predictions are precise predictions for the content and strength of higher order multipoles. In this study, we investigate the degree to which the constraint predictions accurately describe the data.

This is the first time that waveform models incorporating higher order modes from numerical relativity have been applied to an observed gravitational wave signal [6]. This summer, I will be applying these improved signal models to other events observed in O3.

C.   Gravitational waveform modelling

The three waveform families currently used to accurately model gravitational waves for binary systems are the phenomenological waveforms, effective-one-body waveforms, and numerical relativity surrogates. The phe-

nomenological and effective-one-body waveforms model the inspiral, merger, and ringdown of the gravitational wave signal[19]; however, the numerical relativity surrogates are typically limited before the merger and ringdown [13].

D.   Phenomenological models

The phenomenological waveforms focus on modeling the inspiral, merger, and ringdown (IMR) of a gravitational wave signal without providing equations of motions for the black hole dynamics [18]. The phenomenological waveform model is typically created in the frequency domain which makes it computationally quick to evaluate for data analysis applications [18]. The newest edition of the phenomenological waveform models are IMRPhenomPv3HM and IMRPhenomXPHM. IMRPhenomPv3HM and IMRPhenomXPHM tracks precession and includes higher modes [18].

E.   Effective-one-body models

Effective-one-body (EOB) waveform models have calibrated to numerical relativity simulations as well as waveforms from black hole perturbation theory [19]. These waveform models have been utilized to constructed frequency domain, phenomenological models for the inspiral, merger and ringdown of a binary black hole coalescence. The newest EOB model, SEOBNRv4PHM, includes both spin precession and higher modes [19]. The numerical relativity waveforms which have been used to calibrate EOB waveforms included mass ratios $q = 1 - 4$ and dimensionless spins, $\chi_{1,2}$ up to 0.9 [19].

F.   Numerical relativity surrogate models

Numerical relativity simulations are able to accurately model the complex morphology of binary black hole mergers; however, the simulations are computationally expensive. Numerical relativity based surrogates are an alternative approach as they are substitute models for the outputs of these simulations. These models use numerical relativity simulated waveforms to reconstruct underlying phenomenology [13]. The newest numerical relativity surrogate mode, NRSur7dq4 begins ~20 orbits before merger and includes all $\ell \leq 4$ spin-weighted spherical harmonic modes [13]. The seven parameters in the precessing binary black hole system are the mass ratio ($q = m_1/m_2$) where $m_1 \geq m_2$ and the two spin vectors χ_1 and χ_2 where χ_1 represents the heavier black hole [13]. To generate a waveform in the time domain using the NRSur7dq4 model, parameters are required to calculate the waveform, like all other models. These inputs include, the system's mass ratio, dimensionless spin vector of the two black holes, total mass of the total black

hole, maximum ℓ index for modes to use, reference frequency, initial frequency, distance, and sample rate.

G. Phenomenology of higher-order modes

To explore the detectability of higher order modes in varying parameter space, in Fig. 3, I show the real part of the $(\ell, m) =$ (2,1), (2,2), (3,2), (3,3), and (4,4) modes in the time-domain. Fig. 3 was generated using the NR-Sur7dq4 model with parameters located in Table. I. We see that in both the time and frequency-domain (Fig. 4), the (2,2) mode has the highest amplitude while the features in the (3,3) mode occur at 1.5 times the frequency as for the (2,2) mode and the (4,4) mode, with the lowest amplitude, is at twice the frequency of the (2,2) mode
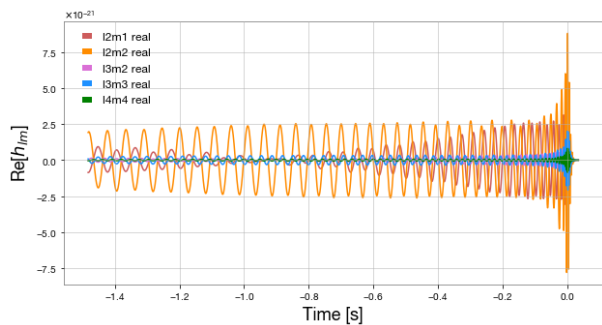

FIG. 3. The real part of the (2,1), (2,2), (3,2), (3,3), and (4,4) modes of the NRSur7dq4 surrogate model waveform. To produce this figure, all waveforms used a $q=4$, $\chi_1=$[-0.2, 0.4, 0.1], and $\chi_2 =$[-0.5, 0.2, -0.4]. Each waveform has been time shifted so its total amplitude appears at $t = 0$.

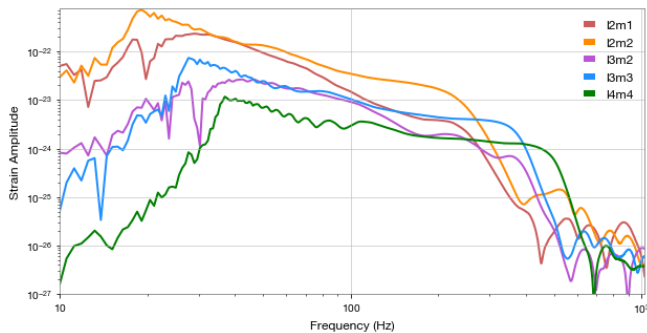FIG. 4. The (2,1), (2,2), (3,2), (3,3), and (4,4) modes of the NRSur7dq4 waveform in the frequency domain.

To analyze gravitational wave signals, it is often helpful to convert the waveform to the frequency-domain. This can be accomplished using a fast Fourier transform. In order to mitigate numerical artefacts, I apply a Tukey window function to the time-domain data before performing the fast Fourier transform. This windowing function reduces the effects of spectral leakage and Gibbs phenomena [20].

TABLE I. Parameters used to evaluate all waveforms

q	χ_1	χ_2,	$M_\odot$	d (Mpc)	ℓ_{max}
4	[-0.2, 0.4, 0.1]	[-0.5, 0.2, -0.4]	70	100	4

Fig. 4 shows that as the mode of the waveform increases, the amplitude decreases. The oscillations located at lower and higher frequencies are likely an artefact of signal processing and Gibbs phenomenon which could be further reduced with a more careful choice of window function. Looking at the orange line representing the (2,2) mode, the inspiral occurs between the minimum simulated frequency, 20 to ∼200Hz. The plunge and merger then appears at 200-250Hz where the curve flattens. We also note that the frequency behaves accordingly to m which means $m = 4$ is one and a half the frequency of $m = 3$ and twice the frequency of $m = 2$.

III. COMPARISON OF HIGHER-MODE MODELS FOR GW190412

In this section, I compare two waveform models, IMR-PhenomPv3HM and SEOBNRv4PHM, using parameters from GW190412. NRSur7dq4 could not be used in this comparison since it was not listed as a waveform model in the posterior sample file.

A. IMRPhenomPv3HM

I compared four IMRPhenomPv3HM waveforms using three sets of GW190412's posterior samples for source properties [15] and one with parameters from the GW190412 Fact Sheet [21]. Posterior samples are important to include in the parameters of the waveform since they provide a more accurate representation of the signal which corresponds to a given model and detector. Fig. 5 shows that the waveform using the parameters from the Fact Sheet is the most different from the other three; however, as all four waveforms approach merger and ringdown, the phases agree.

B. SEOBNRv4PHM

I proceeded to compared four SEOBNRv4PHM waveforms using three sets of GW190412's posterior samples for source properties[15] and one with parameters from the GW190412 Fact Sheet [21]. Fig. 6 shows similar waveform behavior as in Fig. 5 where the four waveforms have disagreement in the inspiral stage; however, as they all approach merger and ringdown, the phases agree. The waveform using the parameters from the GW190412 Fact Sheet (represented in orange) is visibly more different from the other three waveforms. Using posterior samples is a much more accurate way to generate waveforms

since they are obtained using Bayesian parameter estimation methods which infer the sources' of astrophysical properties [12].
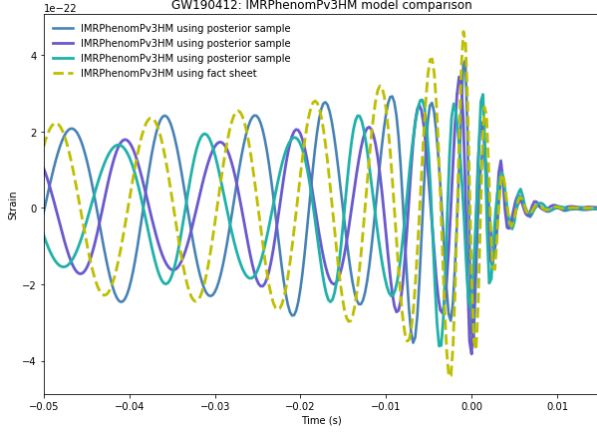

FIG. 5. Time-domain waveforms of IMRPhenomPv3HM using three sets of posterior samples for the source parameters [15] and one waveform with parameters from the GW190412 Fact Sheet [21].
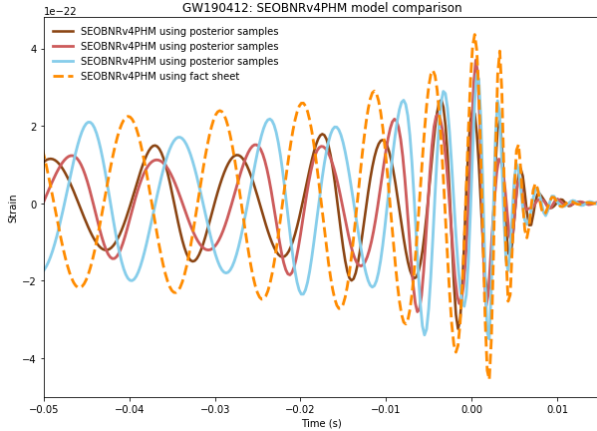

FIG. 6. Time-domain waveforms of IMRPhenomPv3HM using three sets of posterior samples for the source parameters [15] and one waveform with parameters from the GW190412 Fact Sheet [21].

C. IMRPhenomPv3HM and SEOBNRv4PHM

The next comparison is between the two waveforms produced by IMRPhenomPv3HM and SEOBNRv4PHM using two sets of the posterior samples for GW190412. What makes this comparison different is the inclusion of the antenna response function. Gravitational wave detectors produce a time series $h(t)$ which contains the response function (F_+ and $F_\times$) of the detector to each polarisation (h_+ and $h_\times$) which can be described as

$$h(t) = F_+(\theta, \phi, \psi)h_+(t) + F_\times(\theta, \phi, \psi)h_\times(t). \quad (2)$$

For this comparison, I used PyCBC's methods [22] to calculate the projection onto the antenna patterns for the LIGO Livingston detector. Additional parameters such as the source's sky location (θ, ϕ) and the corresponding polarization angle are needed (ψ). It is important to transform the two polarisations according to the interferometer antenna patterns because this affects the signal of the gravitational wave as seen by the detector. As shown in Fig. 7, the time domain waveforms for IMRPhenomPv3HM and SEOBNRv4PHM show visible differences in the shape of the waveform models. The varying amplitude of the waveform suggests that the two have different spin modulation effects. We also observe that as the two waveform models approach merger, they agree well in phase.

In order to determine how well IMRPhenomPv3HM and SEOBNRv4PHM agree with one another, it is often useful to compute the inner product $(h_1|h_2)$ of the two models. I generated 100 IMRPhenomPv3HM and SEOBNRv4PHM waveforms with parameters given by the 12,513 posterior samples. With IMRPhenomPv3HM defined as h_1, SEOBNRv4PHM as h_2, LIGO Livingston's PSD as $S_n(f)$, and the Fourier transform of $h_1(f)$ as $\tilde{h}_1(f)$, the noise-weighted inner product between $(h_1|h_2)$ is given by

$$(h_1|h_2) = \int_{f_0}^{f_1} \frac{\tilde{h}_1(f)\tilde{h^*}_2(f)}{S_n(f)} df \quad (3)$$

where $f_0 = 20$ Hz and $f_1 = 4096$ Hz [23]. The normalized overlap, which is bounded between zero and one, is defined as

$$\mathcal{O}(h_1, h_2) = \frac{(h_1|h_2)}{(h_1|h_1)^{1/2}(h_2|h_2)^{1/2}} \quad (4)$$

By producing a histogram of the 100 evaluated overlaps as shown Fig. 8's left historgram, we can see that overall, $\mathcal{O} \geq 0.9$ across the parameter space of GW190412. This result tells us that despite the different waveform shapes in the time domain, there is a strong overlap between the waveforms. We note the two waveforms often had $0.75 \leq \mathcal{O} \leq 0.87$ which demonstrates that both waveforms can overlap well with the data yet not strongly with each other.

The iteration of 100 evaluated overlaps was computed twice more. The first instance, as shown in middle histogram in Fig. 8, was to show the normalized overlap between the 100 IMRPhenomPv3HM waveform pairs computed using 100 different posterior samples. The second instance compares the normalized overlap between 100 SEOBNRv4PHM waveform pairs which are also computed using 100 different posterior samples. The middle histogram in Fig. 8 shows that the overlap is mostly high, $\mathcal{O} \geq 0.92$ while the left histogram in Fig. 8 shows
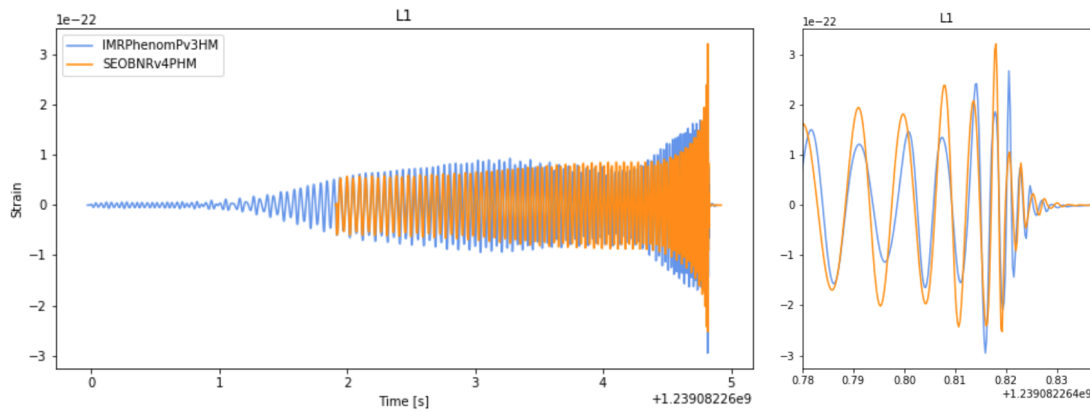
FIG. 7. Time-domain comparison of GW190412 using SEOBNRv4PHM and IMRPhenomPv3HM with posterior samples for the source parameters [15]. Each waveform is projected onto the antenna patterns for the LIGO Livingston detector.
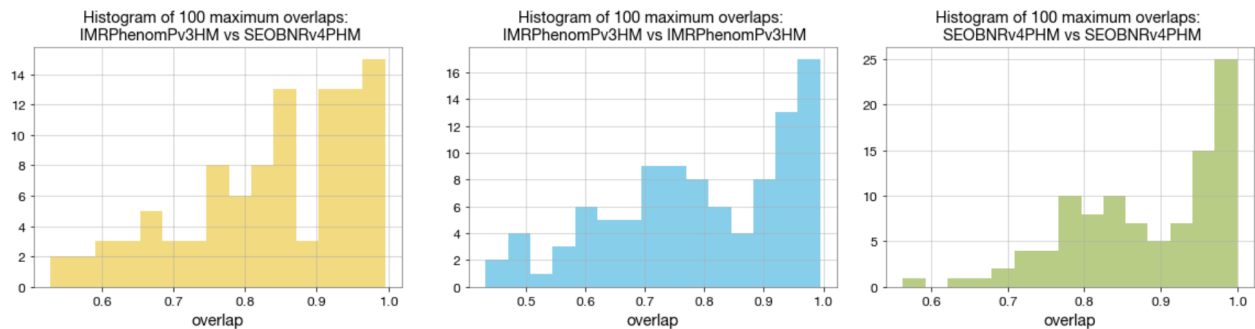

FIG. 8. Three histograms of 100 normalized overlaps between different waveforms. Left: normalized overlaps between IMRPhenomPv3HM and SEOBNRv4PHM waveforms. Middle: normalized overlaps between IMRPhenomPv3HM waveforms. Right: normalized overlaps between SEOBNRv4PHM waveforms. All parameters used to generate the waveforms come from the GW190814 posterior samples for source properties [15].

that the overlap is slight higher, $\mathcal{O} \geq 0.93$. These results provide evidence that the waveform models produce consistent outcomes when using different posterior samples from gravitational wave signals.

IV. FUTURE WORK

A way to confirm that the overlap of SEOBNRv4PHM and IMRPhenomPv3HM is within the statistical errors

would be to generate an event with a high SNR, e.g., SNR = 100. Using Bilby, we can compare the waveform models and produce their corresponding histograms to show a strong overlap. Another task I will be working on is to use Bilby to compute a Bayes factor for simulated gravitational wave signals with and without higher order modes, and study the differences in the estimated parameters (as in Fig. 2). By accomplishing this, we will be able to demonstrate the ability to distinguish the presence of higher order modes quantitatively.

[1] LIGO Scientific Collaboration, J. Aasi, and *et al.*, Advanced LIGO, Classical and Quantum Gravity **32**, 074001 (2015), arXiv:1411.4547 [gr-qc].

[2] F. Acernese, M. Agathos, K. Agatsuma, D. Aisa, N. Allemandou, A. Allocca, J. Amarni, P. Astone, G. Balestri, G. Ballardin, and et al., Advanced virgo: a second-generation interferometric gravitational wave detector, Classical and Quantum Gravity **32**, 024001 (2014).

[3] B. P. Abbott, R. Abbott, T. D. Abbott, and *et al.* (LIGO Scientific Collaboration and Virgo Collaboration), GWTC-1: A gravitational-wave transient catalog of compact binary mergers observed by LIGO and Virgo during the first and second observing runs, Phys. Rev. X **9**, 031040 (2019).

[4] T. L. S. Collaboration and T. V. Collaboration, Sensitivity Achieved by the LIGO and Virgo Gravitational Wave

Detectors during LIGO's Sixth and Virgo's Second and Third Science Runs (2012), arXiv:1203.2674 [gr-qc].

[5] The LIGO Scientific Collaboration and Virgo Collaboration, Gravitational-wave candidate event database, https://gracedb.ligo.org/superevents/public/O3/.

[6] The LIGO Scientific Collaboration, the Virgo Collaboration, R. Abbott, T. D. Abbott, S. Abraham, F. Acernese, K. Ackley, and *et al.*, GW190412: Observation of a binary-black-hole coalescence with asymmetric masses (2020), arXiv:2004.08342 [astro-ph.HE].

[7] B. Abbott, R. Abbott, T. Abbott, M. Abernathy, F. Acernese, K. Ackley, C. Adams, T. Adams, P. Addesso, R. Adhikari, and et al., Tests of general relativity with gw150914, Physical Review Letters **116**, 10.1103/physrevlett.116.221101 (2016).

[8] B. P. Abbott, R. Abbott, T. D. Abbott, S. Abraham, F. Acernese, K. Ackley, C. Adams, R. X. Adhikari, V. B. Adya, C. Affeldt, and et al., Binary black hole population properties inferred from the first and second observing runs of advanced ligo and advanced virgo, The Astrophysical Journal **882**, L24 (2019).

[9] The LIGO Scientific Collaboration and Virgo Collaboration, B. P. Abbott, R. Abbott, T. D. Abbott, and *et al.*, A gravitational-wave measurement of the hubble constant following the second observing run of advanced ligo and virgo (2019), arXiv:1908.06060 [astro-ph.CO].

[10] R. Abbott, T. D. Abbott, S. Abraham, F. Acernese, K. Ackley, C. Adams, R. X. Adhikari, V. B. Adya, C. Affeldt, M. Agathos, and et al., Gw190814: Gravitational waves from the coalescence of a 23 solar mass black hole with a 2.6 solar mass compact object, The Astrophysical Journal **896**, L44 (2020).

[11] Gravitational-wave open data workshop #3, https://www.gw-openscience.org/s/workshop3.

[12] G. Ashton, M. Hübner, P. D. Lasky, C. Talbot, K. Ackley, S. Biscoveanu, Q. Chu, A. Divakarla, P. J. Easter, B. Goncharov, and et al., Bilby: A user-friendly bayesian inference library for gravitational-wave astronomy, The Astrophysical Journal Supplement Series **241**, 27 (2019).

[13] V. Varma, S. E. Field, M. A. Scheel, J. Blackman, D. Gerosa, L. C. Stein, L. E. Kidder, and H. P. Pfeiffer, Surrogate models for precessing binary black hole simulations with unequal masses, Physical Review Research **1**, 10.1103/physrevresearch.1.033015 (2019).

[14] C. M. Biwer, C. D. Capano, S. De, M. Cabero, D. A. Brown, A. H. Nitz, and V. Raymond, Pycbc inference: A python-based parameter estimation toolkit for compact binary coalescence signals, Publications of the Astronomical Society of the Pacific **131**, 024503 (2019).

[15] Sample release for gw190412, https://dcc.ligo.org/LIGO-P190412/public/.

[16] B. S. Sathyaprakash and B. F. Schutz, Physics, Astrophysics and Cosmology with Gravitational Waves., Living Rev. Relativ. **12**, 10.12942 (2009).

[17] J. B. Hartle, *Gravity: An Introduction to Einstein's General Relativity*, illustrate ed. (Benjamin Cummings).

[18] L. London, S. Khan, E. Fauchon-Jones, C. García, M. Hannam, S. Husa, X. Jiménez-Forteza, C. Kalaghatgi, F. Ohme, and F. Pannarale, First higher-multipole model of gravitational waves from spinning and coalescing black-hole binaries, Physical Review Letters **120**, 10.1103/physrevlett.120.161102 (2018).

[19] S. Ossokine, A. Buonanno, S. Marsat, R. Cotesta, S. Babak, T. Dietrich, R. Haas, I. Hinder, H. P. Pfeiffer, M. Pürrer, C. J. Woodford, M. Boyle, L. E. Kidder, M. A. Scheel, and B. Szilágyi, Multipolar effective-one-body waveforms for precessing binary black holes: Construction and validation (2020), arXiv:2004.09442 [gr-qc].

[20] Wikipedia, Gibbs phenomenon — Wikipedia, the free encyclopedia, http://en.wikipedia.org/w/index.php?title=Gibbs%20phenomenon&oldid=959691031 (2020), [Online; accessed 07-July-2020].

[21] GW190412 Fact Sheet, https://dcc.ligo.org/public/0167/G2000545/006/GW190412_Factsheet_Final.pdf.

[22] Antenna Patterns and Projecting a Signal into the Detector Frame, https://pycbc.org/pycbc/latest/html/detector.html.

[23] B. J. Owen, Search templates for gravitational waves from inspiraling binaries: Choice of template spacing, Physical Review D **53**, 6749–6761 (1996).